Experimental Study on Flow Control Characteristics of Synthetic Jets over a Blended Wing Body Configuration

Byunghyun Lee[1)], Minhee Kim[1)] , Chongam Kim[1)] , Taewhan Cho[2)], Seol Lim[3)], and Kyoung Jin Jung[4)]

[1)] *Seoul National University, Seoul, South Korea*
[2)] *Korea Aerospace Research Institute, Daejeon, South Korea*
[3)] *Hanwha Coporation, , Daejeon, South Korea*
[4)]*Agency for Defense Development, Daejeon, South Korea*

This paper presents experimental investigations on the characteristics of synthetic jets over blended wing body configuration. Flow control experiments were performed by using piezoelectrically driven synthetic jet under various flow conditions. In the first step, baseline characteristics of blended wing body configuration were analyzed when synthetic jet was off. Pressure distribution and separated-flow region on the wing surface were examined by changing the angle of attack. Flow control experiments were carried out by synthetic jet to demonstrate the flow control performance in the post-stall regime. Comparative studies were also conducted for a stalled condition. Aerodynamic coefficient was examined by changing synthetic jet operating condition, such as jet oscillation frequency and jet module locations. Based on various comparisons, it was observed that synthetic jet operating conditions have significantly influence on the development of leading-edge vorticies, that is to say, flow control performance of synthetic jet.

Key Words: synthetic jet, flow separation control, blended wing body

Nomenclature

α	: angle of attack
C_d	: drag coefficient
C_l	: lift coefficient
f	: oscillation frequency of synthetic jet
U_∞	: freestream velocity

1. Introduction

The control of flow separation has been one of the most promising methods for increasing the aerodynamic performance of future aircrafts. Among the many flow control methods, synthetic jets have been regarded as an efficient way to control various separated regions. Synthetic jets periodically transport momentum flux from a jet exit to an outside region with less energy consumption[1)]. In addition intermittent blowing/suction has been shown to be highly effective at flow control and vortex suppression[2,3)]. The flow control performances of synthetic jets have been studied by both experimental and numerical methods. Kim and Kim[4)] numerically investigated the frequency-dependent flow control mechanisms of synthetic jets on an airfoil and proposed multi-location synthetic jets in order to mitigate the unstable flow structures of a high-frequency jet. Kim *et al.*[5)] demonstrated that flow control using synthetic jets improves the aerodynamic performance of tilt-rotor UAV (Unmanned-Aerial-Vehicle) airfoils under various flight conditions. Kim *et al.*[6)] also showed how a circular exit array can be an efficient way to control the widely separated flow region. The aforementioned studies have shown the potential of synthetic jets in improving aerodynamic performance. However, studies on the flow control capability of synthetic jets are not sufficient, especially regarding the control of a massive separated-flow region on an aircraft configuration in a post-stall regime.

The purpose of this current work is to study the active flow control capability of the synthetic jet system to prevent flow separation on a blended wing body configuration. In the first step, the baseline characteristics of a blended wing body were analyzed when the synthetic jet was off. The pressure distribution and separated-flow region on the wing surface were examined by changing the angle of attack. Stall characteristics were explained by the physics of leading-edge vortices and vortex breakdown. Additionally, synthetic jet flow control experiments were carried out by synthetic jet to demonstrate the flow control performance in the post-stall regime.

2. Experimental Procedure

In order to verify the flow control capability of the synthetic jet, comparative experiments were conducted in a stalled condition. The schematic of piezoelectrically driven actuators for the present experiments is shown in Fig. 1a. The jet momentum generation is based on the principle of volume change in the middle cavity by two piezoelectric diaphragms. The exterior of the synthetic jet module is presented in Fig. 1b. The basic components are made out of acrylic parts, and the piezoelectric diaphragm is installed on both sides of the cavity. The detailed operating condition of the synthetic jet can be found in Ref. 7-8, as well as input voltage amplitude and oscillation frequency.

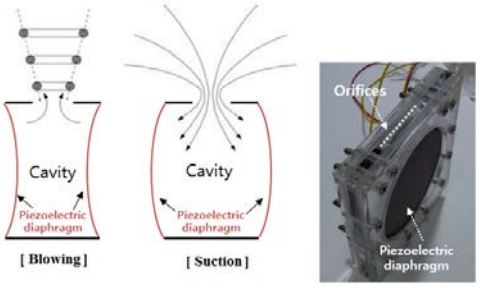

Fig. 1. Principle of dual-diaphragm actuator

Figure 2 shows the wind tunnel setup using the blended wing body model with a 1.184 m chord and 2 m span. Synthetic jet actuators (7 modules on each wing) were installed to prevent leading-edge stall at high angles of attack. All actuators were operated with the same voltage amplitude (V_{pp} = ± 180 V) and oscillation frequency (f = 200 Hz). Static pressure tap arrays were located along the upper surface on the wing. The experiments were then conducted in a subsonic wind tunnel that had a test section of 4 m × 3 m at the KARI (Korea Aerospace Research Institute). The turbulence intensity was less than 0.1 %. And the freestream velocity was 20 m/s. Static pressure taps were installed on the different wing sections with the forces and moments acquired via an external six-component balance. Since flow fluctuations were in separated regions, all pressure data were time-averaged over a period of 10 seconds. The strong suction effect on the top surface created by leading-edge vortices were analyzed by experimental data, like pressure distribution along the spanwise direction and lift coefficient, as shown in Fig. 3.

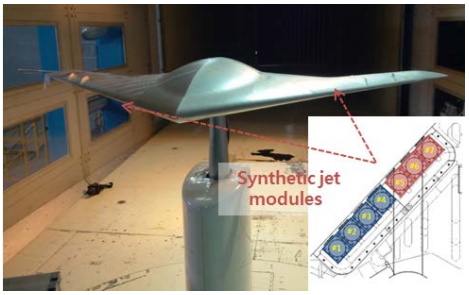

Fig. 2. Wind tunnel test setup

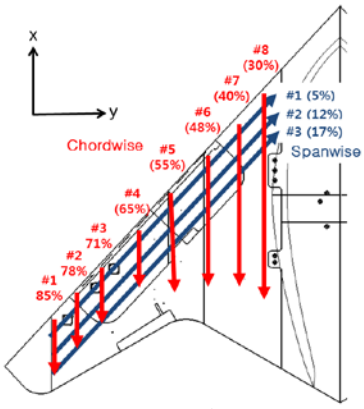

Fig.3 Location of pressure taps

3. Results and Discussions

3.1. Baseline analysis

Studies on the flow characteristics of the blended wing body configuration were performed by changing the angle of attack. Figures 4-6 present aerodynamic forces, which were acquired by an ernal balance. The C_l curve increases linearly before the stall angle (α = 10 degrees) while the lift gradient begins to decrease. The C_d curve remains low before the stall angle and increases drastically after it.

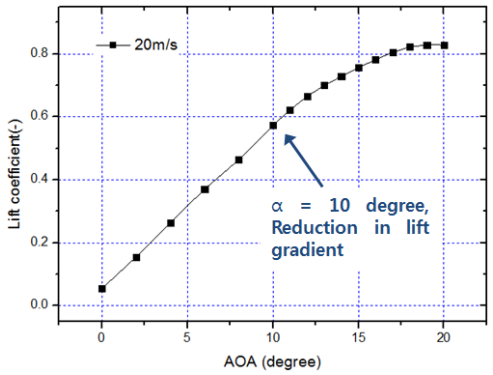

Fig. 4. Lift coefficient curve

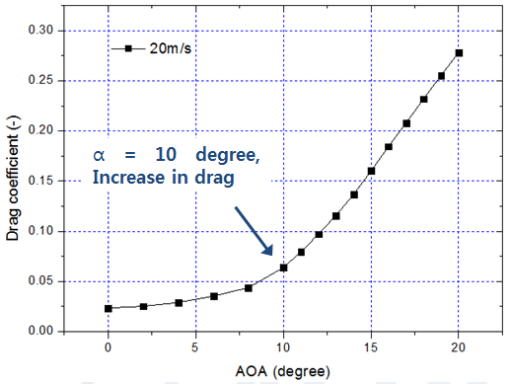

Fig. 5. Drag coefficient curve

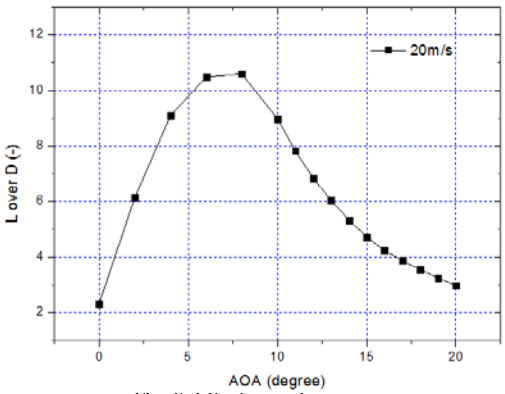

Fig. 6. Lift-drag ratio curve

Figures 7-9 present the flow field using tufts visualization. Before the stall angle, there is mostly attached flow on the wing surface except at the wing tip (Fig. 7). At the initial stall angle, a vortex breakdown occurs along the leading edge and tufts in that region vibrate irregularly (Fig. 8). At the deeper stall angle, the vortex breakdown region and the separated-flow region are merged into each other (Fig. 9).

Though not presented here, the separated-flow region expanded greatly as the angle of attack increased. Finally, most of the wing became fully separated at α = 20 degrees.

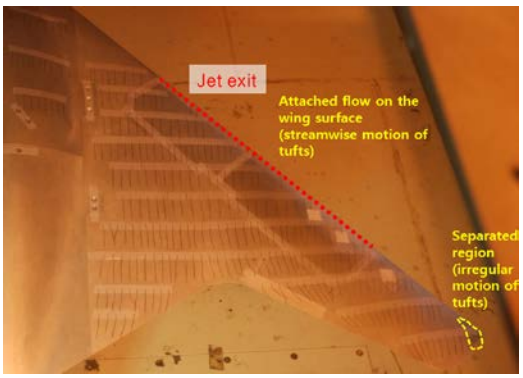

Fig. 7. Tufts visualization (α = 8 degrees)

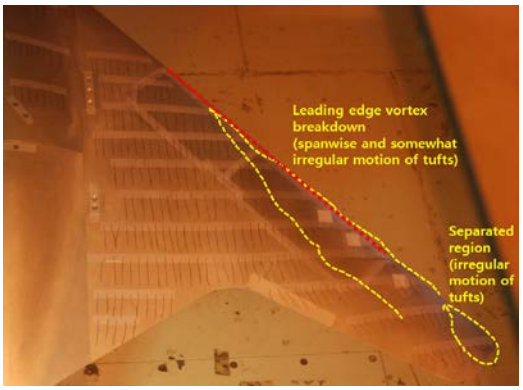

Fig. 8. Tufts visualization (α = 10 degrees)

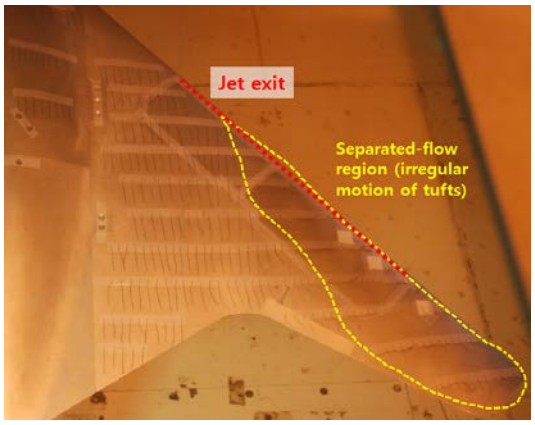

Fig. 9. Tufts visualization (α = 12 degrees)

Figures 10-12 present the spanwise C_p distribution near the leading-edge. The initiation of vortex breakdown can be identified by a suction peak in the spanwise C_p distribution. The leading-edge vortices are known to be a source of high energy, relatively high-vorticity flow[9]. Therefore, the static pressure on the top surface is reduced near the leading-edge. Before the stall angle (α = 8 degrees in Fig. 10-11), C_p distribution along the spanwise direction is nearly constant so that the suction peak is not seen, which means that the spanwise flow near leading-edge is weak. At stall angle (α = 10 degrees in Fig. 10-11), a noticeable suction peak is seen near the leading-edge. By the same token, the leading-edge vortex breakdown starts to occur, as shown in Fig. 8. After a deeper stall (α = 12-16 degrees in Fig. 10-12), the suction peak moves toward the inboard area and its range is expanded to the 3rd line. From the aforementioned results, the vortex breakdown near the leading-edge can be explained by the strength and the position of the suction peak.

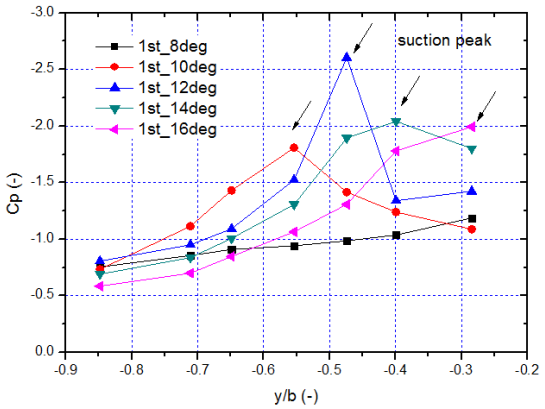

Fig. 10. Spanwise C_p distribution (1st line)

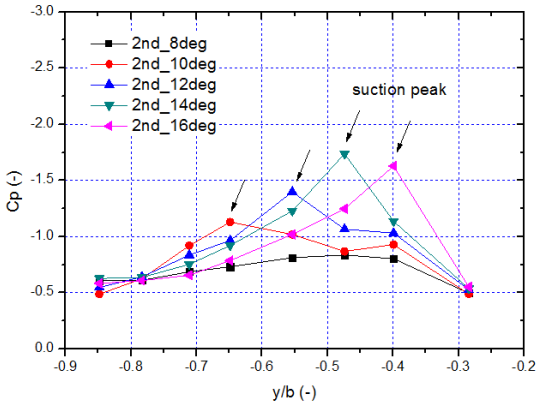

Fig. 11. Spanwise C_p distribution (2nd line)

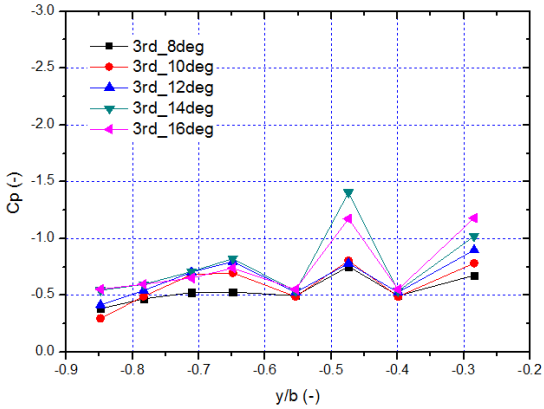

Fig. 12. Spanwise C_p distribution (3rd line)

3.2. Synthetic jet-on

3.2.1 All-actuators-on condition

Referring to the results in Chapter 3-1, the flow separation characteristics on a blended wing body are closely related to the leading-edge vortex breakdown. The leading-edge vortices create a strong suction on the top surface near the leading-edges. The suction effect of the leading-edge vortices, acting to increase the normal force, consequently increases the

lift on the delta wing[9]. However, our main objective in flow separation control is to get a high lift-to-drag in the post stall regime. Therefore, a strategy is needed to solve the flow control performance in the leading-edge vortices.

In order to examine the overall flow control performance of a synthetic jet, all synthetic jet modules near the leading-edge were operated in the post-stall regime. Figure 13 shows the increment of lift and drag coefficient in the post-stall regime. The Flow control performance mainly contributed to the decrement of drag, as shown in Fig. 13. As a result, the lift-to-drag ratio is substantially improved above the stall angle, as stated in Fig. 14. Since both lift and drag are increased by the suction effect caused by the leading-edge vortex, the leading edge vortex has to be treated carefully to increase the overall performance in the post-stall regime.

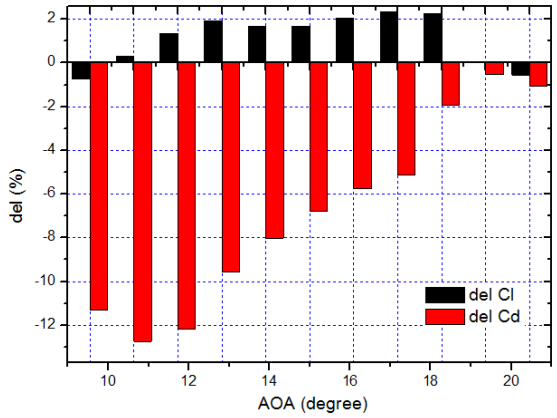

Fig. 13. Increment of C_l and decrement of C_d in the stall regime

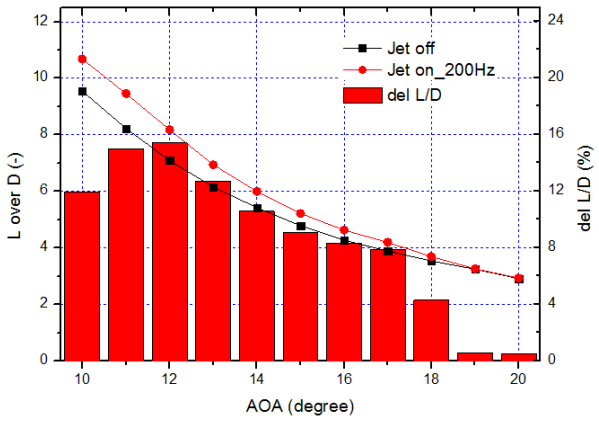

Fig. 14. Comparison of C_l/C_d curve and increment of C_l/C_d

The flow control mechanism in the post-stall regime is analyzed by using the flow field and C_p distribution. Among the post-stall angles, α = 10 and 12 degrees are selected by flow control performance. α = 10 degrees is the stall initiation angle, and α = 12 degrees is the angle which shows the best increment of C_l/C_d.

Figure 15 represents the qualitative effect of the synthetic jet at α = 10 degrees. When the synthetic jet is off (Fig. 15a), tufts near the leading-edge vibrate somewhat irregularly and so their direction spanwise. The tuft's direction near the leading-edge implies the direction of leading-edge vortex. The leading-edge vortex breakdown is shown by the irregular motion of tufts. When the synthetic jet is on (Fig. 15b), the spanwise flow and the separated-flow near the leading-edge are eliminated. As a result, the tuft direction is recovered so that it is in the streamwise direction. This means that the leading-edge vortex breakdown is suppressed by the effect of the synthetic jet momentum.

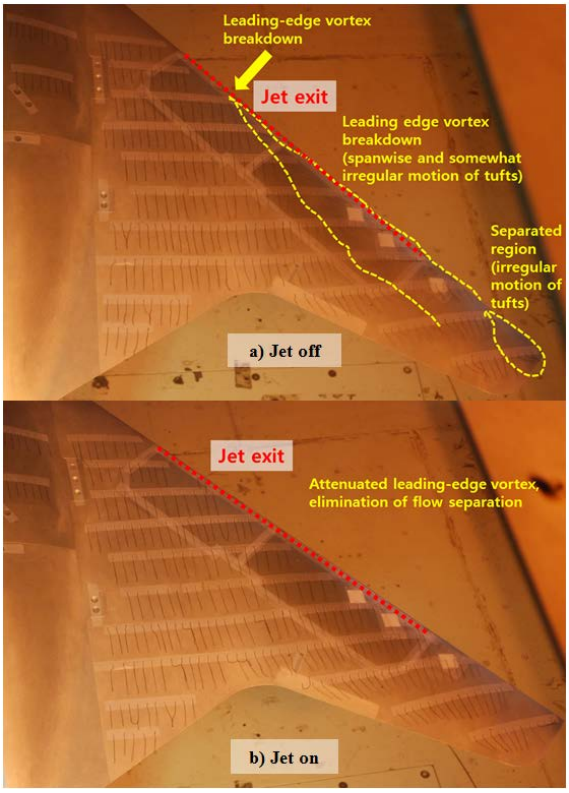

Fig. 15. Qualitative effect of synthetic jet (α = 10 degree)

Figure 16 presents the spanwise C_p distribution at α = 10 degrees. Referring to the baseline data in Figs. 10-11, a noticeable suction peak is seen at the stall angle. When the synthetic jet is on, the suction peak is suppressed. The weakness of the suction peak is consistent with the flow field in Fig. 15b. Figure 17 shows a chordwise C_p distribution α = 10 degrees, which shows a separated-flow region near the leading-edge similar to the airfoil section. The separated-flow region is normally observed by a constant C_p region in two-dimensional flow. Like the 2-D flow, the separated-flow region elimination on each chordwise section is observed by the recovery of the C_p slope. The flow control effect mainly appears at the outboard region of the jet exit (#1-6 line), because the leading-edge vortex and mixed-jet momentum flow inboard to outboard. The leading-edge area in the #5 line has an especially high recovery for pressure loss. On the other hand, the synthetic jet merely affects the inboard area (#7-8 line). The synthetic jet has a negative influence on the #3 and #4 lines whose C_p slopes are lower than that in the baseline case.

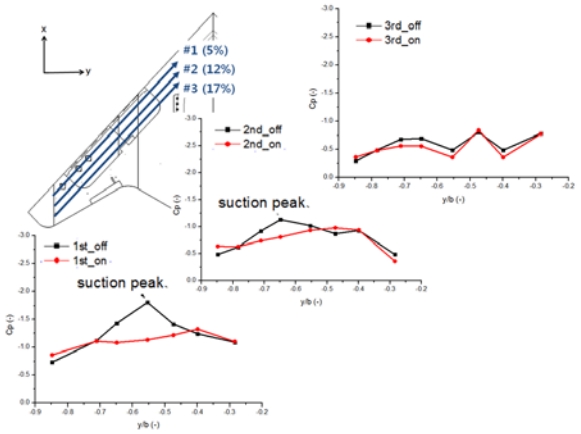

Fig. 16 Spanwise C_p distribution (α = 10 degrees)

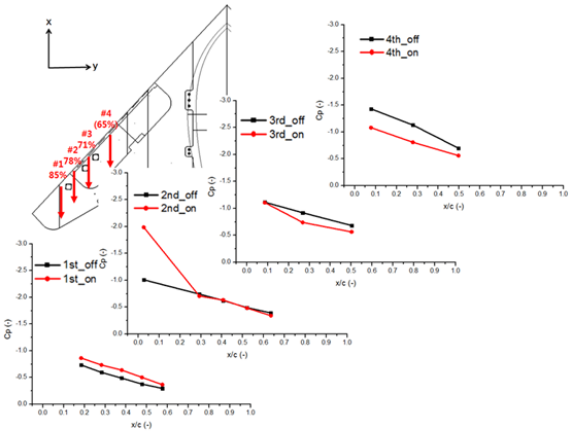

a) 1st – 4th line

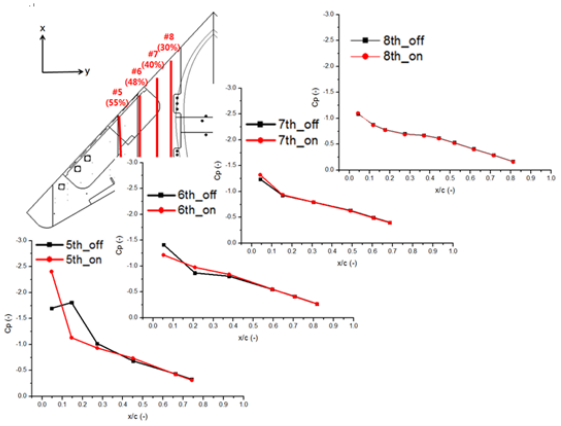

a) 5th – 8th line

Fig. 17. Chordwise C_p distribution (α = 10 degrees)

This means that the uniform supply of jet momentum near the leading-edge may reduce the flow control performance at specific areas. From this perspective, the selective supply of jet momentum can be an alternative to solving a local degradation of the synthetic jet.

Figure 18 shows tuft visualization in the case of α = 12 degrees. The separated-flow region is not completely removed by the synthetic jet as compared to the result of α = 10 degrees that is shown in Fig. 15. Instead, the location of the leading-edge vortex breakdown moves outboard and the separated-flow area is reduced. Figure 19 presents a spanwise C_p distribution at α = 12 degrees. The suction peak is not completely eliminated, compared to the result of α = 10 degrees as shown in Fig. 16. Instead, its strength is reduced and its position moves outboard. Figure 20 shows the chordwise C_p distribution at α = 12 degrees. Comparing this to the results of α = 10 degrees (Fig. 17), the synthetic jet positively affects it through a wide area, where the C_p slopes are generally recovered throughout the #1-5 lines. However, the C_p slope at the #6 line is decreased by the synthetic jet.

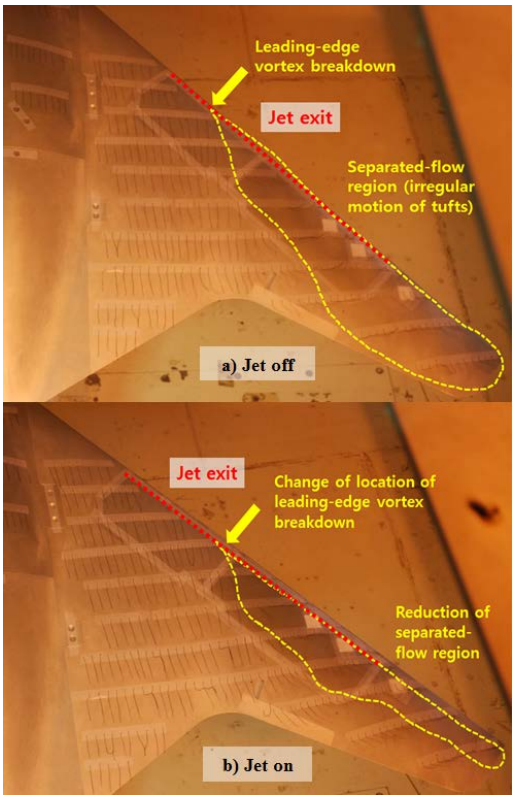

Fig. 18. Qualitative effect of synthetic jet (α = 12 degrees)

The flow characteristics of all-actuators-on experiment demonstrate that the synthetic jet is effective at controlling the leading-edge vortex breakdown near the leading-edge. These results are caused by the changing position of the leading-edge vortex breakdown and jet momentum of the synthetic jet. As the angle of attack increases, the position of the leading-edge vortex breakdown moves inboard and its strength increases (Figs. 10-12). Thus, the synthetic jet affects through a wide area (#1-5 lines) at α = 12 degrees because the location of the leading-edge vortex breakdown is located inside that of α = 10 degrees. At the same time, the leading-edge vortex breakdown happens at the inner inboard region and the separated-flow region becomes larger as the angle of attack increases. However, the jet momentum of the synthetic jet is fixed at f = 200 Hz, so the same amount of jet momentum as α = 10 degrees condition is not enough to eliminate the suction peak at that. Thus, the flow control performance of α = 10 degrees is shown more clearly than that of α = 12 degrees.

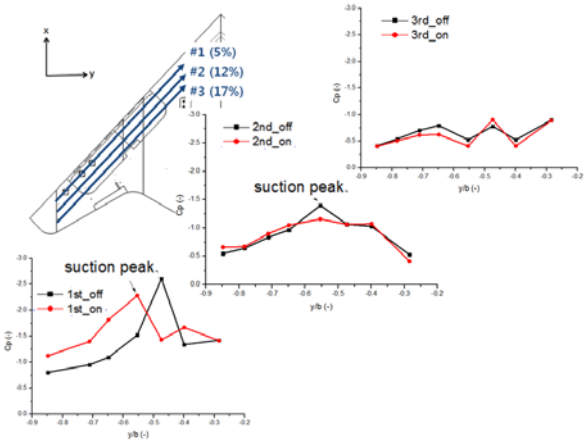

Fig. 19. Spanwise C_p distribution (α = 12 degrees)

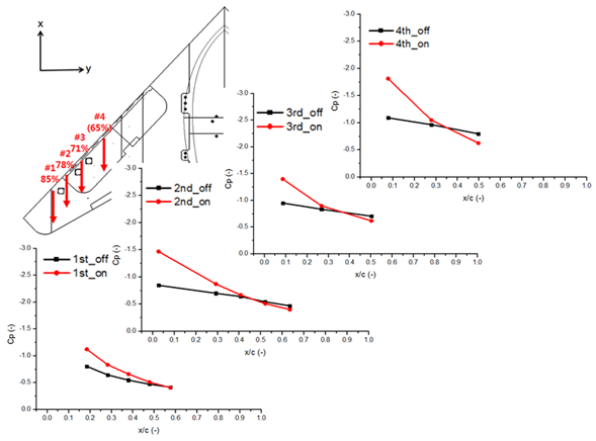

a) 1st – 4th line

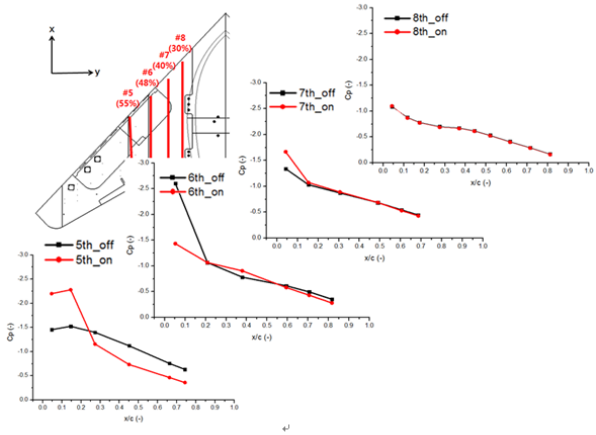

b) 5st – 8th line

Fig. 20. Chordwise C_p distribution (α = 12 degrees)

On the other hand, a uniform supply of jet momentum near the leading-edge has a limitation because the jet momentum adversely affects some areas. Therefore, the selective supply experiment of jet momentum was designed to overcome the traditional method of uniform supply at the leading-edge. The experimental result is explained in the following section.

3.2.2 Selective-actuators-on condition

In order to find an effective flow control method according to the leading-edge vortex breakdown position, the flow control experiments were performed by changing the number of synthetic jet modules. Figure 21 shows the increment of C_l/C_d depending on the number of synthetic jet modules. Figure 21a (total increment of C_l/C_d) indicates the overall quantity of flow control and Fig. 21b (increment of C_l/C_d per module) refers to the flow control performance efficiency. When the flow control is strongest at the lowest power consumption, there is efficient flow control. Therefore, the selective operating condition is important in considering the practical use and power consumption of synthetic jet modules. As shown in Fig. 21a, the more synthetic jet module operates the higher overall flow control performance.

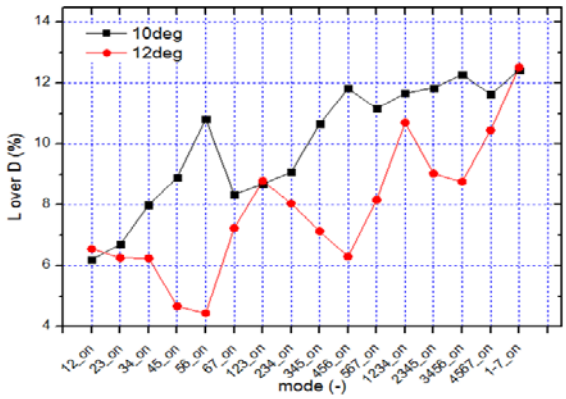

a) Total increment of C_l/C_d

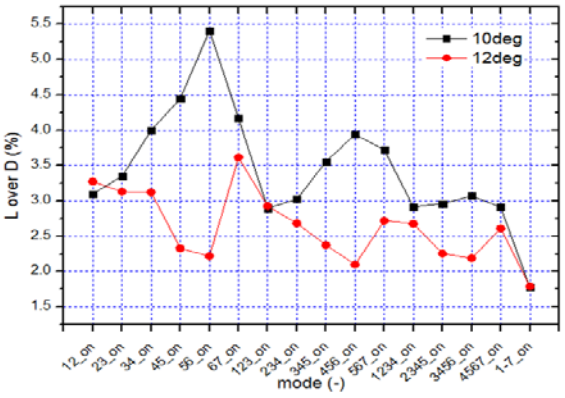

b) Increment of C_l/C_d per module

Fig. 21. Increment of C_l/C_d

However, as the number of synthetic jet modules increases, the efficiency is generally reduced, as shown in Fig. 21b. Furthermore, as we focus on the results of two-modules in Fig. 21b, the relationship between the synthetic jet positions and the leading-edge vortex breakdown is identified. Table 1 quantitatively compares the flow control performance according to the number of synthetic modules. The first and second cases of synthetic jet module numbers are summarized in Table 1. When α = 10 degrees, the first case commonly includes #5 and #6 modules, while the second case has #4 and #5 modules. When α = 12 degrees, even though the first and second cases are shifted a small quantity of C_l/C_d increment, all cases include #1 and #2 or #6 and #7 modules. From this perspective, the relationship between the leading-edge vortex breakdown position and synthetic jet modules is analyzed.

Table 1. Quantitative comparison of flow control performance

module	α = 10 degrees		α = 12 degrees	
	First	Second	First	Second
2	**#5#6**	**#4#5**	**#6#7**	**#1#2**
3	#4#**5#6**	#3**#4#5**	**#1#2**#3	#5**#6#7**
4	#3#4**#5#6**	#2#3**#4#5**	**#1#2**#3#4	#4#5**#6#7**

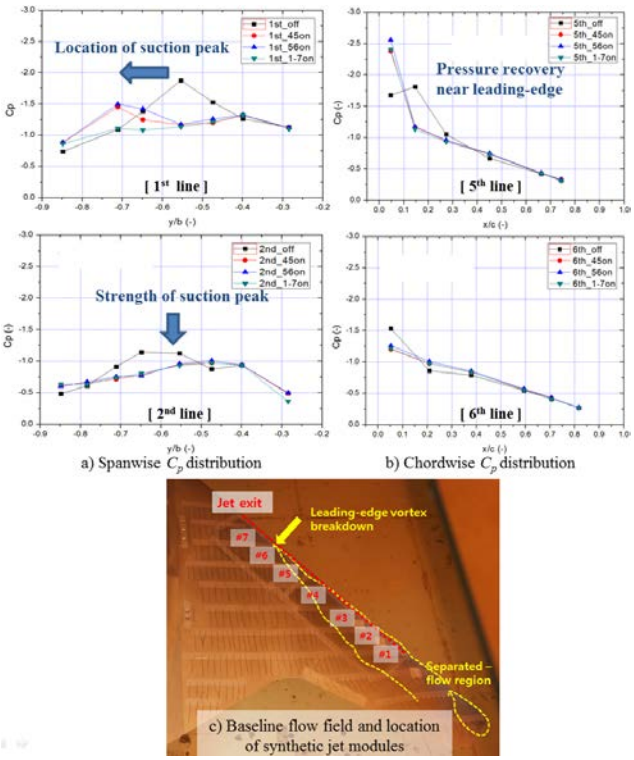

Fig. 22. C_p distribution and synthetic jet position (α = 10 degrees)

Figures 22 and 23 show the C_p distribution and the position of synthetic jet modules. The results of the two-module cases in Table 1 and the result of all-module case in Chap. 3.2.1 are compared to one another. When α = 10 degrees, the locations of suction peak at the #1 line are moved outboard by the two-module actuation (Fig 22a). This movement of the suction peak is inferior to the elimination of the suction peak in an all-actuators-on case, but the strength of the suction peak is equally suppressed at the #2 line. Moreover, the chordwise C_p distribution (Fig 22b) indicates that the recovery of the C_p slope can be achieved by two-module case. When α = 12 degrees, the results of the #6 and #7 modules and the results of #1 and #2 modules are similar with respect of the amount of C_l/C_d increment (Fig. 21). However, the flow control mechanisms of those cases are different, as shown in Fig. 23. Because the #6 and #7 modules are located near the leading-edge vortex breakdown, these modules contribute to the suction peak movement toward outboard at the 1st line (Fig. 23a). On the other hand, the #1 and #2 modules in the separated-flow region do not directly affect the movement of the suction peak, and cause pressure recovery at the outboard area instead (y/b = 0.75 – 0.85 in 1st line, Fig. 23a). The chordwise C_p distribution (Fig. 23b) also compares the characteristics of flow control according to the synthetic jet position. In the case of the #6 and #7 modules, the pressure recovery level at the 5th line is similar to an all-actuators-on case. On the other hand, in the case of the #1 and #2 modules, the pressure recovery level at the 5th line is lower than that of the all-actuators-on case. However, a beneficial effect is shown considering the pressure loss at the 6th line that is observed in an all-actuator-on case.

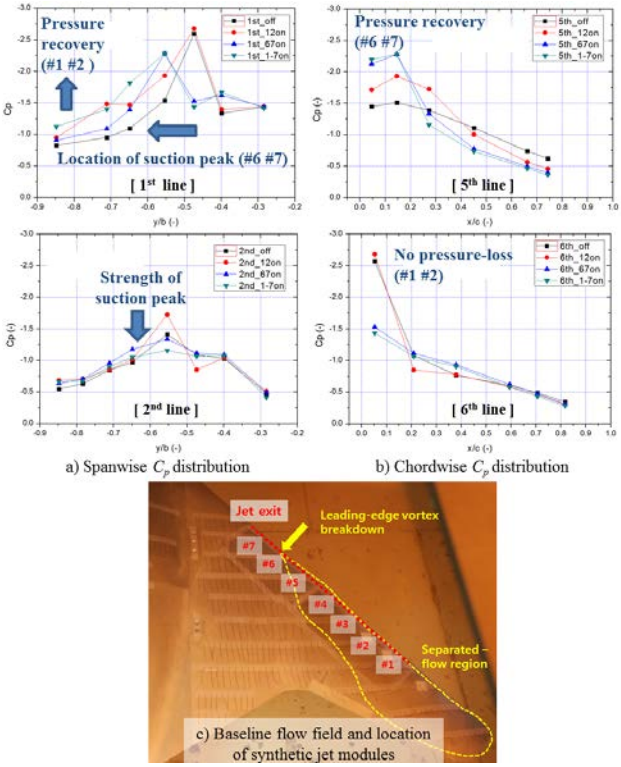

Fig. 23. C_p distribution and synthetic jet position (α = 12 degrees)

From these results it is possible to note that the flow control mechanism is changed by the position of synthetic jet modules, or the supply of jet momentum. When there is initial stall (α = 10 degrees), the leading-edge vortex breakdown starts mildly and the separated-flow region is small. Thus, the direct supply of jet momentum at the leading-edge vortex breakdown is effective. Therefore, as the further synthetic jet modules are away from the leading-edge vortex breakdown (suction peak), the less likely synthetic jet control separated-flow region is identified, as shown in Fig. 21. When there is deeper stall (α = 12 degrees), the leading-edge vortex breakdown happens strongly at the inner inboard region and the separated-flow region is large. Thus, the direct supply of jet momentum at the suction peak contributes to the movement and suppression of the leading-edge vortex breakdown. The supply of jet momentum at the separated-flow region of outboard brings about pressure recovery at the outboard region.

4. Conclusions

Flow characteristics of synthetic jet over a blended wing body configuration have been investigated by the experimental method. In the first step, the baseline analysis of the blended wing body configuration was performed while changing the angle of attack when the synthetic was off. Through various aerodynamic data and flow visualization, the leading-edge vortex breakdown was observed to mainly affect the separated-flow physics in the post-stall regime. In the second step, the flow control strategy was established by baseline data. The full operation of synthetic jet modules near the leading-edge effectively suppressed the development of the leading-vortex breakdown and considerably reduced the separated-flow region at the initial stall stage. However, a uniform supply of jet momentum locally yields pressure loss at the leading-edge. A selective operation of the jet module was investigated to enhance the effectiveness of synthetic jet. At the initial stall stage, a pinpoint operation of the synthetic jet effectively controlled the strength of the leading-edge vortex breakdown, even though a relatively small amount of jet momentum was supplied. For deeper stall, a direct supply of jet momentum at separated-flow region was also effective at controlling the starting point of the leading-edge vortex breakdown. From these results, it was concluded that the strategic operation of the synthetic jet over a blended wing body was an efficient alternative to controlling the separated-flow region in a post-stall regime while considering power consumption.

Acknowledgments

This research was supported by Defense Acquisition Program Administration and Agency for Defense Development (UC100031JD). The authors also appreciate the financial and administrative help from the Institute of Institute of Advanced Aerospace Technology.

References

1) Greenblatt, D., and Wygnanski, I. J., “The control of flow separation by periodic oscillation,” Progress in Aerospace Sciences, Vol. 36, 2000, pp. 487-545.
2) Rao, D. M., "Pneumatic Concept for Tip-Stall Control of Cranked-Arrow Wings," Journal of Aircraft,Vol 31,No. 6,1994,pp. 1380-1386.
3) Trebble, W. J. G., "Exploratory Investigation of the Effects of Blowing from the Leading Edge of a Delta wing," ARC R&M 3518, April, 1966.
4) Kim, S., and Kim, C., “Separation control on NACA23012 using synthetic jet,” Aerospace Science and Technology, Vol. 13, 2009, pp. 172-182.
5) Kim, M., Kim, S., Kim, W., Kim, C. and Kim, Y., “Flow Control of Tilt rotor Unmanned-Aerial-Vehicle Airfoils Using Synthetic Jets,” Journal of aircraft, Vol. 48, 2011, pp. 1045-1057.
6) Kim, W., Kim, C., and Jung, J., “Separation Control Characteristics of Synthetic Jets Depending on Exit Configuration,” AIAA JOURNAL, Vol. 50, 2012.
7) Lee, B. Kim, M., Lee, J., Kim, C., “Separation Control Characteristics of Synthetic Jets with Circular Exit Array”, 6th AIAA Flow Control Conference, AIAA-2012-3050, New Orleans, Louisiana, 25-28 June, 2012.
8) Lee, B. Kim, M., Lee, J., Kim, C., “Closed-loop Active Flow Control of Stall Separation using Synthetic Jets”, 31st AIAA Applied Aerodynamics Conference, AIAA-2013-2925, San Diego, California, 24-27 June, 2013.
9) Anderson, J. D., “Fundamental of Aerodynamics”, 2nd edition, 1991, p. 360.